Nano Energy 41 (2017) 66–74

Contents lists available at ScienceDirect

Nano Energy

journal homepage: www.elsevier.com/locate/nanoen

Full paper

Enhanced sodium storage capability enabled by super wide-interlayer-spacing MoS_2 integrated on carbon fibers

Changtai Zhao[a,b], Chang Yu[a,*], Mengdi Zhang[a], Qian Sun[b], Shaofeng Li[a], Mohammad Norouzi Banis[b], Xiaotong Han[a], Qiang Dong[a], Juan Yang[a], Gang Wang[a], Xueliang Sun[b,*], Jieshan Qiu[a,*]

[a] State Key Lab of Fine Chemicals, School of Chemical Engineering, Liaoning Key Lab for Energy Materials and Chemical Engineering, Dalian University of Technology, Dalian 116024, PR China

[b] Department of Mechanical and Materials Engineering, University of Western Ontario, London, ON, Canada, N6A 5B9

ARTICLE INFO

Keywords:
Sodium-ion batteries
MoS_2
Pseudocapacitance
Long cycle life
Sodium-ion hybrid capacitors

ABSTRACT

Developing advanced electrode materials for effective pseudocapacitive charge storage is one of effective strategies to enhance the rate capability and cycling stability of sodium ion storage devices. Herein, we fabricate MoS_2 nanoflowers with super wide interlayer spacing (nearly twice as large as that of the original MoS_2) supported on carbon fibers (named as E-MoS_2/carbon fibers) and demonstrate its superior electrochemical performances as flexible and binder-free anodes for sodium-ion batteries (SIBs) and sodium-ion hybrid capacitors (SIHCs). Grafting MoS_2 nanoflowers onto the carbon fiber networks not only ensures the fast electron transfer, but also endows it with flexible feature. The super wide interlayer spacing of MoS_2 nanoflowers can not only decrease the ion diffusion pathways and resistance, but also increase their available and accessible active surface area, thus guaranteeing the rapid mass transport. Also, it can accommodate the large internal strain during discharge/charge processes. Benefiting from these combined structure merits, the E-MoS_2/carbon fibers electrodes deliver an ultralong cycling stability up to 3000 cycles and the superior rate capacity of 104 mA h g^{-1} at 20 A g^{-1}, which just takes *ca.* 18.7 s to fully charge/discharge. When further employed as the anode for SIHCs, it delivers high energy and power densities due to the high pseudocapacitive charge storage of the super wide interlayer spacing E-MoS_2/carbon fibers.

1. Introduction

Recently, sodium-ion batteries (SIBs) have triggered tremendous interests as the alternatives to lithium-ion batteries (LIBs) owing to the advantages such as low cost and large resource availability of sodium [1–4]. And there have been extensive researches on the development of the high-rate and long-life anode materials for SIBs to meet the requirements of high power density devices such as fast charging portable electronics and electric vehicles [5–10]. Nevertheless, the present SIBs still suffer from the inferior rate capability and poor cycling life due to the sluggish kinetics of diffusion-controlled battery reaction along with the large volume expansion [11–13]. However, how to alleviate the severe kinetics barriers of SIBs related to the slow solid-state ion diffusion processes and to accommodate the accompanying volume change still remain a great challenge [14,15].

Pseudocapacitive energy storage, a kind of charge storage mode based on the superficial faradic reaction mechanism, possesses the battery-like high energy density and double layer capacitors-like high power density [16]. Combining capacitance into battery system would be a promising and potential approach to achieving the high power density and long life span in sodium storage. In order to achieve improved charge storage behavior via pseudocapacitance in sodium storage, three key points need to be considered: (1) rapid mass transport in terms of short ion diffusion pathways and low ion diffusion resistance; (2) fast electron transfer within the whole electrode matrix; (3) highly available and accessible active surface area [9,17]. The rational configuration of advanced electrode materials with high pseudocapacitive charge storage is required to meet the high rate capability and long cycling stability of sodium storage. Meanwhile, the development of this kind of materials may represent and guide a new frontier in achieving fast energy storage technology [16,18,19]. Moreover, compared with LIBs, the larger ionic radius of Na^+ and sluggish reaction kinetics make it more difficult and challenging to seek appropriate anode materials to meet these requirements [20–22].

* Corresponding authors.
E-mail addresses: chang.yu@dlut.edu.cn (C. Yu), xsun9@uwo.ca (X. Sun), jqiu@dlut.edu.cn (J. Qiu).

http://dx.doi.org/10.1016/j.nanoen.2017.08.030
Received 21 June 2017; Received in revised form 15 August 2017; Accepted 17 August 2017
Available online 19 August 2017

MoS_2, a typical graphite-like layered structure with S-Mo-S motifs stacked together by Van der Waals forces, has attracted extraordinary attention as the anode material for rechargeable SIBs [23]. The well-defined layered structure with a large interlayer spacing (0.62 nm) is in favor of initial Na^+ intercalation. While inherent chemical properties of MoS_2 feature a followed chemical conversion process, which can eventually accommodate a large amount of Na^+ [24,25]. Nevertheless, when used as anode material for SIBs, big bulk and thick plate-shaped MoS_2 suffers from significantly increased diffusion distance of Na^+ and large internal strain during discharge/charge processes, resulting in cracking of electrode materials [26]. Meanwhile, MoS_2 also suffers from a low inherent electronic conductivity, which will further cause serious polarization and low electrode material utilization efficiency [27]. Therefore, tailoring and optimizing the nanostructure of MoS_2 are vital and effective to increase its mass and electron transportation, thus achieving high pseudocapacitive charge storage. For example, constructing the MoS_2 with open structure and the super wide interlayer spacing can significantly enhance the rate of mass transport and releases the internal strain during the discharge/charge processes [28]. Additionally, coupling MoS_2 with highly conductive 3D carbon substrate in a harmonious manner will further ensure the fast electron transfer [29,30]. Combined with all these desirable merits together, high-rate and long-life sodium storage can be achieved.

Herein, we report a high-rate and long-life sodium storage enabled by expanded and super wide interlayer spacing MoS_2 supported on carbon fibers (E-MoS_2/carbon fibers) via increasing the pseudocapacitive charge storage. Benefiting from the enhanced mass transport and electron transfer, the as-made E-MoS_2/carbon fibers deliver a superior rate capacity of 104 mA h g^{-1} at an ultrahigh current density of 20 A g^{-1} and an ultralong cycling stability up to 3000 cycles due to its high pseudocapacitive charge storage. The electrochemical analysis shows that the ratio of the capacitive contribution even reaches as high as 89.4% at a scan rate of 2 mV s^{-1}. When being made to sodium-ion hybrid capacitors (SIHCs) with the commercial activated carbon (AC) as the counter electrode, it also delivers a high energy density of 54.9 Wh kg^{-1}. The superior electrochemical performance of E-MoS_2/carbon fibers is attributed to (1) the open structure of MoS_2 nanoflowers that is capable of increasing the contact area between the electrode materials and electrolyte and shortening the ion diffusion pathways; (2) the expanded and super wide interlayer spacing of MoS_2 that can decrease the ion diffusion resistance and increase the available and accessible active surface area; (3) the interwoven carbon fiber networks as the flexible substrate that enable the smooth electron transfer for the gifted MoS_2 nanoflowers.

2. Experimental section

2.1. Synthesis of carbon fibers

The polyacrylonitrile (PAN)-based carbon fibers were prepared by a typical electrospinning method with PAN as the precursor, followed by annealing process. Firstly, the polymer solution of 10 wt% PAN in N, N-Dimethylformamide (DMF) was electrospun from a syringe tip to a rotating metal collector (aluminium foil, at a drum rotation rate of 300 rpm) under a highly supplied voltage of 22 kV. Then, the obtained PAN-based fiber precusors were aged at a rate of 1 °C min^{-1} from room temperature to 280 °C, and kept at this temperature for 2 h in air. Then, the atmosphere was changed to N_2, and the temperature was heated to 800 °C at a ramping rate of 5 °C min^{-1} and kept at this temperature for 1 h. After that, the carbon fibers were infiltrated into 60 mL of HNO_3 solution (69.2 wt%) and kept at 100 °C for 1 h in 80 mL of Teflon-line stainless-steel autoclave. Finally, the pre-treated carbon fibers were washed and dried for further use.

2.2. Synthesis of the E-MoS_2/carbon fibers

Typically, 0.2 g of $(NH_4)_6Mo_7O_{24}{\cdot}4H_2O$, 0.18 g of thiourea, and 0.55 g of polyvinylpyrrolidone (Mw ≈ 55000) were dissolved into 30 mL of deionized water under strong stirring. Then, 20 mg of pre-treated carbon fibers were infiltrated into the prepared solution and kept at 190 °C for 18 h in 40 mL of Teflon-line stainless-steel autoclave. After cooling down, the precursors were washed with a large amount of deionized water and ethanol, and dried at room temperature. Finally, the sample was heated at 500 °C for 3 h with a ramping rate of 5 °C min^{-1} in N_2, yielding the E-MoS_2/carbon fibers. For comparison, E-MoS_2 and MoS_2/carbon fibers were also synthesized in the absence of carbon fibers and PVP, respectively.

2.3. Materials characterization

The morphology, crystalline structure and composition of the as-made samples were analyzed by scanning electron microscopy (SEM, Hitachi S-4800), transmission electron microscopy (TEM, FEI TF30), powder X-ray diffraction (XRD, Bruker D8 Advance, Cu K α X-ray source).

2.4. Electrochemical measurements

The SIBs performance for the as-made samples was evaluated by using 2032-type coin cells with a voltage window of 0.01–3.0 V. The free-standing carbon fibers and E-MoS_2/carbon fibers can be directly used as the anode after cutting into slices with the diameter of *ca.* 1.0 cm without any auxiliary binders and conductive additives. The coin cells can be assembled with a sodium metal slice, electrolyte (1 M $NaClO_4$ in ethylene carbonate (EC) and diethyl carbonate (DEC) (volume ratio of 1:1) with 10 wt% fluoroethylene carbonate (FEC) additive), a glass fiber separator and a slice of the as-made sample in an argon-filled glovebox. The galvanostatic discharge-charge test was performed on an Arbin battery testing system. The cyclic voltammetry (CV) and electrochemical impedance spectroscopy (EIS) tests were carried out by using a Bio-logic VSP electrochemical workstation with a voltage widow of 0.01–3.0 V at different scan rates and the frequency range between 100 kHz and 0.01 Hz at open circuit potential, respectively. All the electrochemical performance was tested at the temperature of 25 ± 1 °C. The average areal loading of the active material was *ca.* 1 mg cm^{-2}, and the specific capacity was calculated based on the total mass of the active material.

The AC electrodes were prepared by casting the slurry consisting of 80 wt% commercial activated carbon (BET2000, ACS MATERIAL), 10 wt% carbon black and 10 wt% polyvinylidene difluoride (PVDF) binder in N -methyl-2-pyrrolidone (NMP) onto an Al foil current collector, followed by drying at 80 °C for 12 h in vacuum oven. The electrolyte and separator of the SIHCs were the same to those of the SIBs as mentioned above. Before the assembly of SIHCs, the E-MoS_2/carbon fibers anodes were cycled for five cycles at the current density of 100 mA g^{-1} in SIBs. The current density and energy density were calculated based on the total mass of the anode and cathode active materials. The capacitance (C), energy density (E), and power density (P) of SIHCs were calculated based on the followed Eqs. (1)–(3):

$$C = 3.6{\cdot}Q/\Delta V \quad (1)$$

where Q is the discharge capacity (mA h g^{-1}), ΔV is the discharge/charge voltage window.

$$E = 0.5{\cdot}C{\cdot}\Delta V^2 \quad (2)$$

$$P = E/\Delta t \quad (3)$$

where Δt is the discharge time.

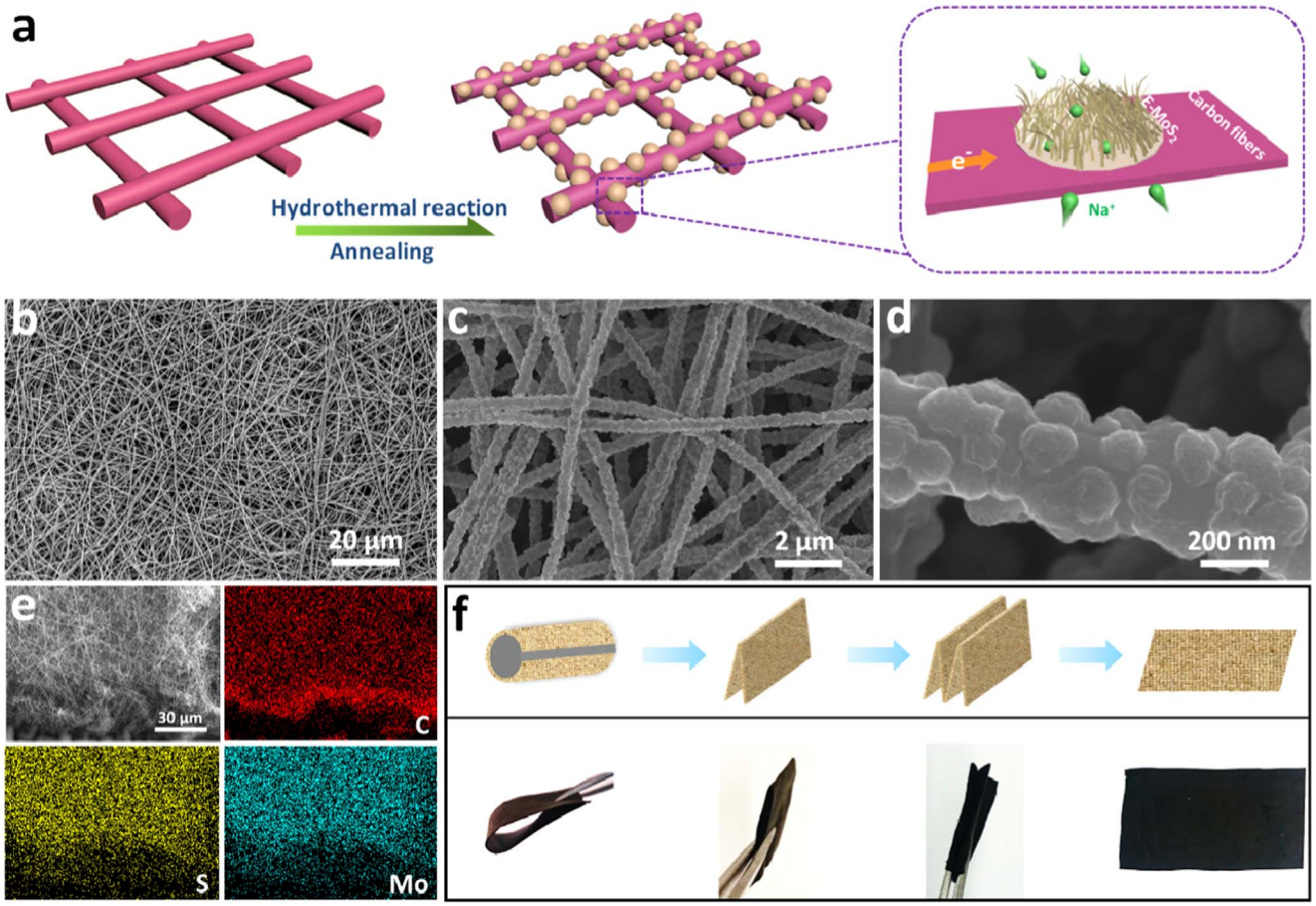

Fig. 1. (a) Schematic illustration for the synthesis of E-MoS_2/carbon fibers. (b-d) SEM images of the E-MoS_2/carbon fibers. (e) SEM image of the E-MoS_2/carbon fibers and the corresponding EDS elemental mapping images. (f) Free-standing and flexible features of the as-made E-MoS_2/carbon fibers.

3. Results and discussion

The architectures made of MoS_2 nanoflowers with expanded and super wide interlayer spacing supported on carbon fibers were synthesized by a polyvinylpyrrolidone (PVP)-assisted hydrothermal reaction and following annealing, of which the schematic illustration is shown in Fig. 1a. The morphology and structure of the as-made samples were investigated by SEM. The representative SEM images of carbon fibers are displayed in Fig. S1, revealing a typically interconnected network structure made of the interwoven electrospinning carbon fibers with an average diameter of 250 nm. And, the architectures can be well inherited after being grafted with MoS_2 nanoflowers, as shown in Fig. 1b. The high-magnification SEM images in Fig. 1c, d and Fig. S2 show that the MoS_2 nanoflowers with an average size of 140 nm are uniformly and densely anchored on the 1D carbon fibers with an intimate and electronic contact, which is in favor of rapid electron transfer during discharge/charge processes [31]. It also can be evidenced by the high conductivity of E-MoS_2/carbon (0.18 S m^{-1}) inheriting from the carbon fibers (0.48 S m^{-1}). The uniform distribution of MoS_2 nanoflowers on carbon fibers can also be evidenced by energy dispersive X-ray spectroscopy (EDS) elemental mapping images (Fig. 1e). Moreover, after a series of severe folds, the E-MoS_2/carbon fibers can be well kept and recovered (Fig. 1f), indicative of the potential and feasibility as free-standing and flexible electrode materials.

The nanostructure of MoS_2 nanoflowers was further analyzed by TEM and high resolution TEM (HRTEM), of which the detailed results are shown in Fig. 2a-c. Fig. 2a, b and Fig. S3 further confirm the uniform distribution of MoS_2 nanoflowers on the surface of carbon fibers and reveal the open structure of MoS_2 nanoflowers, which is in favor of the intimate contact and sufficient interaction between electrode and electrolyte, as well as shortening ion diffusion pathways [32]. The further HRTEM image of E-MoS_2/carbon fibers in Fig. 2c demonstrates that the interlayer spacing of MoS_2 nanoflowers is sufficiently expanded to more than 1.34 nm (much larger than the 0.62 nm of commercial MoS_2). The increased interlayer spacing can obviously reduce the ion diffusion resistance and increase the available and accessible active surface area to electrolyte [28,33]. For comparison, the composites of the normal MoS_2 grafted on carbon fibers (MoS_2/carbon fibers) were also fabricated in the absence of PVP, and the representative SEM and TEM image are shown in Fig. S4. It can be found that the MoS_2 in MoS_2/carbon fibers featuring a sheet-shaped structure is uniformly fixed on the surface of carbon fibers. The HRTEM image further demonstrates that the interlayer spacing of the MoS_2 is *ca.* 0.68 nm, which is much less than that of the MoS_2 with super wide interlayer spacing in E-MoS_2/carbon fibers.

The XRD patterns shown in Fig. 2d and Fig. S5 suggest that the as-made E-MoS_2/carbon fibers exhibits the characteristic diffraction peaks of carbon and MoS_2, suggesting the successful configuration. Compared with the (002) peak of commercial MoS_2, a large shift of 8.1° is presented on the as-made pure MoS_2 with super wide interlayer spacing (E-MoS_2), which further confirms that the interlayer spacing of the as-made MoS_2 was successfully and sufficiently expanded [28]. The broad (002) characteristic peak of E-MoS_2 indicates a wide range of interlayer spacing. This is also well consistent with the TEM observation results, which will be in favor of the rapid ion diffusion in-between the MoS_2 layers (Fig. 2e). Raman spectra of carbon fibers and E-MoS_2/carbon fibers samples shown in Fig. 2f both exhibit two distinct peaks at 1359 cm^{-1} and 1587 cm^{-1} corresponding to the D-band and G-band of carbon materials, respectively. The characteristic peaks of E-MoS_2/carbon fibers and commercial MoS_2 at 378 cm^{-1} and 403 cm^{-1}

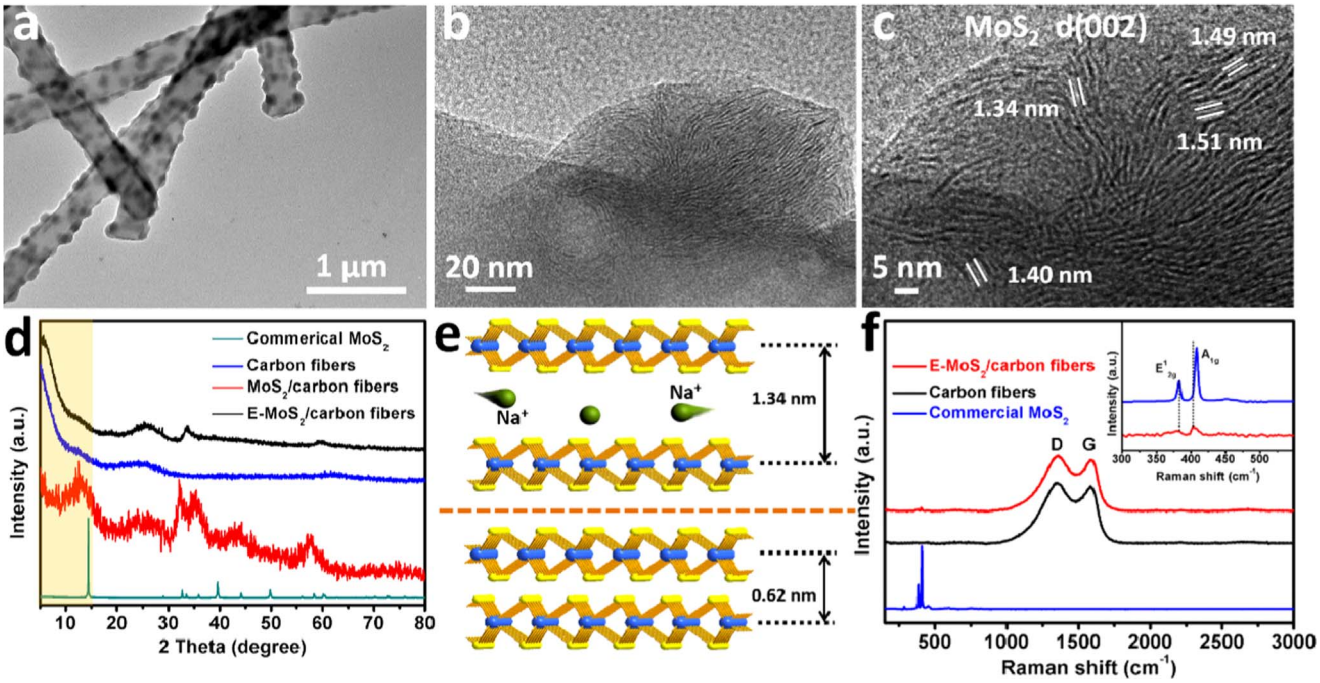

Fig. 2. (a, b) TEM images and (c) HRTEM image of the E-MoS_2/carbon fibers. (d) XRD patterns of the as-made carbon fibers, E-MoS_2/carbon fibers, MoS_2/carbon fibers, and commercial MoS_2. (e) Structural models of the MoS_2 with different interlayer spacings. (f) Raman spectra of the carbon fibers, E-MoS_2/carbon fibers, and commercial MoS_2.

correspond to the in-plane E^1_{2g} and the out-of-plane A_{1g} of MoS_2 with the typical hexagonal layered structure, respectively [34]. Compared with the commercial MoS_2, the A_{1g} characteristic peak has shifted from 408 cm^{-1} for commercial MoS_2 to 403 cm^{-1} for E-MoS_2/carbon fibers. This obvious shift is mainly attributed to the fact that the features of MoS_2 with the expanded interlayer spacing give rise to a diminished interlayer van der Waals force which would result in a stronger out-of-plane vibration. The Raman characterization further confirms that the MoS_2 nanoflowers are successfully coupled onto the carbon fibers matrix.

The local chemical structure and coordination environment of the E-MoS_2/carbon fibers composites were further studied by using X-ray absorption spectroscopy (XAS), and the results are shown in Fig. 3. The Mo K-edge X-ray absorption near edge structure (XANES) spectra of E-MoS_2/carbon fibers and commercial MoS_2 (Fig. 3a) reveal the similar pre-edge and white line features. This also indicates that Mo ions within E-MoS_2/carbon fibers still correspond to the +IV oxidation state [35]. The Fourier-transformed extended X-ray absorption fine structure (EXAFS) spectrum of the commercial MoS_2 (Fig. 3b) exhibits two distinct peaks corresponding to Mo-S and Mo-Mo bonds, respectively, which are attributed to the presence of the nearest neighboring sulfur atoms and Mo atoms around a central Mo atom. The Fourier-transformed spectrum of the as-made E-MoS_2/carbon fibers exhibits the well-developed Mo-S peak and a relatively weak Mo-Mo contribution in comparison to that of commercial MoS_2, indicative of the sufficiently expanded interlayer spacing of MoS_2 within the as-made E-MoS_2/carbon fibers [36]. The thermogravimetric analysis reveals that the ratio of the MoS_2 and carbon fibers in E-MoS_2/carbon fibers composites are 37% and 63%, respectively (Fig. S6).

In view of the above structural and compositional characterization results, the as-made E-MoS_2/carbon fibers can be capable of being an excellent high-power electrode material for sodium storage. Of course, this is mainly attributed to their integrated advantages, including shortened Na^+ diffusion pathways, decreased Na^+ diffusion resistance, and enhanced electron mobility. With this information in mind, the electrochemical performance of the as-made E-MoS_2/carbon fibers was firstly evaluated as a binder-free anode for SIBs. Fig. 4a shows the CV curves of the E-MoS_2/carbon fibers electrode for the first three cycles

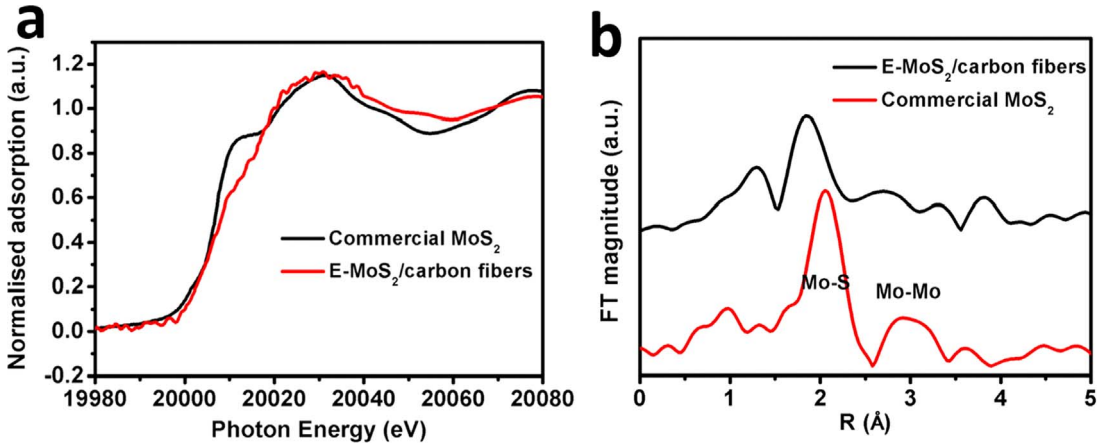

Fig. 3. (a) Mo K-edge XANES spectra and (b) Mo K-edge Fourier-transformed EXAFS spectra of the commercial MoS_2 and E-MoS_2/carbon fibers.

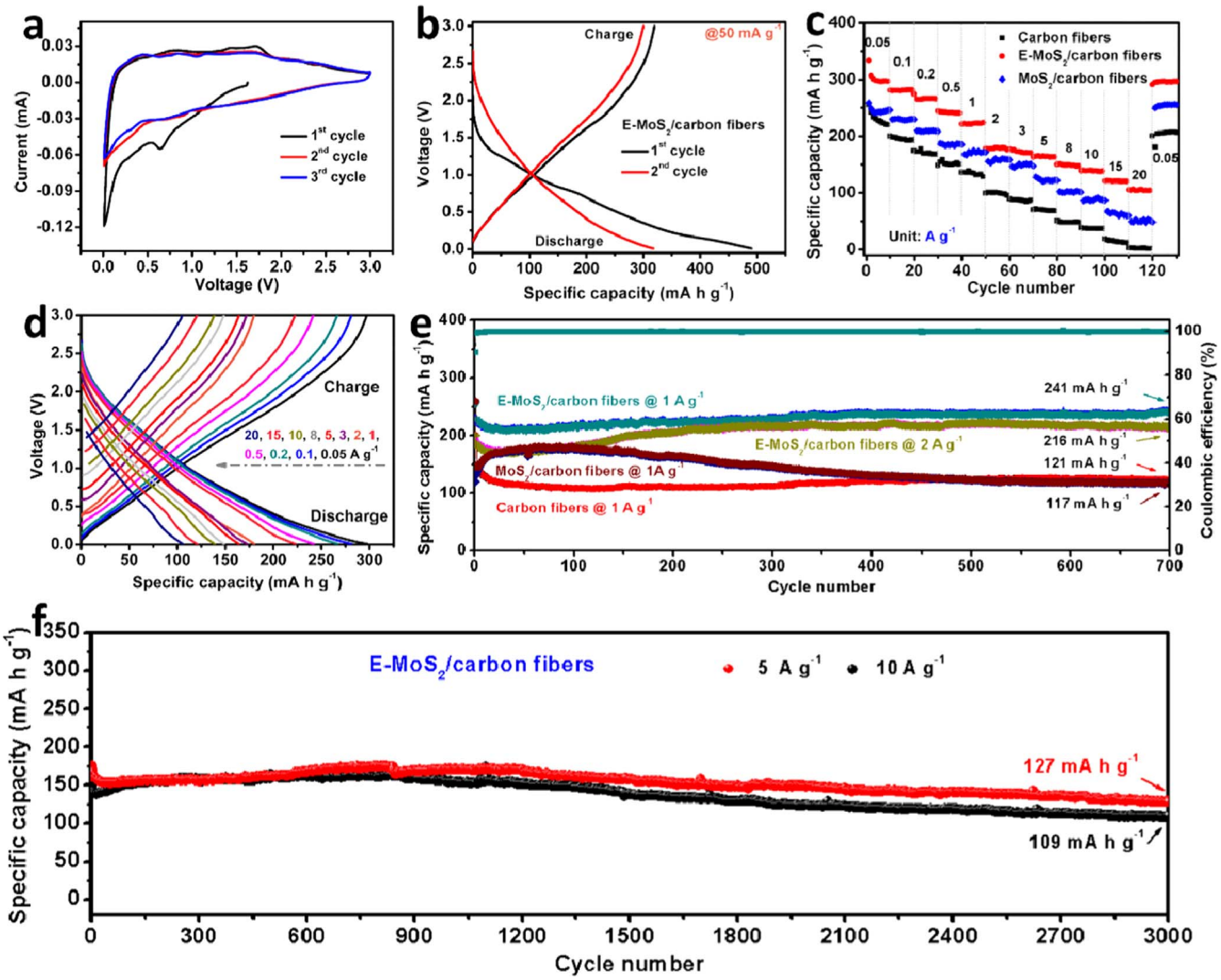

Fig. 4. (a) CV curves of the as-made E-MoS_2/carbon fibers at a scan rate of 0.1 mV s^{-1}. (b) The discharge/charge profiles of the E-MoS_2/carbon fibers at a current density of 50 mA g^{-1}. (c) The rate capability of the E-MoS_2/carbon fibers, MoS_2/carbon fibers and carbon fibers. (d) The galvanostatic discharge/charge profiles of the E-MoS_2/carbon fibers at different current densities. (e) The cycle performance of the E-MoS_2/carbon fibers, MoS_2/carbon fibers and carbon fibers and the corresponding Coulombic efficiencies. (f) The cycle performance of the E-MoS_2/carbon fibers at 5 A g^{-1} and 10 A g^{-1}.

tested at a scan rate of 0.1 mV s^{-1} within a voltage window of 0.01–3.0 V. Only one obviously reductive peak at 0.64 V, corresponding to the formation of the solid electrolyte interface (SEI) layer in the 1st cycle, is observed. The almost overlapping CV curves for the 2nd and 3rd cycles imply the high reversibility and excellent cycling stability of the as-made E-MoS_2/carbon fibers composites in SIBs. Fig. 4b shows galvanostatic discharge/charge profiles of the as-made E-MoS_2/carbon fibers for the first two cycles at a current density of 50 mA g^{-1}. The initial discharge and charge capacities of the E-MoS_2/carbon fibers are 490 mA h g^{-1} and 319 mA h g^{-1}, respectively, corresponding to a Coulombic efficiency of 65.1%. The large irreversible initial capacity loss mainly originates from the formation of the SEI layer on the electrode surface [37,38]. One of effective strategies to alleviate this issue is to choose a suitable electrolyte which can modify the SEI formation [39]. By comparison, the carbon fibers and MoS_2/carbon fibers electrodes just deliver relatively low initial charge capacities of 256 and 259 mA h g^{-1}, respectively (Fig. S7). The rate capability of the as-made E-MoS_2/carbon fibers was also evaluated at different current densities ranging from 0.05 to 20 A g^{-1}, and the results are shown in Fig. 4c. The reversible capacities of the E-MoS_2/carbon fibers are 298, 281, 241, 222, 164, 138, and 104 mA h g^{-1} at current densities of 0.05, 0.1, 0.5, 1, 5, 10, and 20 A g^{-1}, corresponding to the high capacity retention rates of 100%, 94%, 81%, 75%, 55%, 47%, and 35%, respectively (Fig. S8), which are much higher than those values of the carbon fibers and MoS_2/carbon fibers. With the high current density up to 20 A g^{-1}, the battery can be fully charged in *ca.* 18.7 s, which is important for ultrafast charging portable electronics and electric vehicles [40–42]. When the current density was back to 0.05 A g^{-1}, the discharge capacity can still recover to 296 mA h g^{-1}, indicative of the high sustainability. The outstanding rate performance is attributed to the highly electronic conductivity of carbon fiber networks and the rapid mass transport derived from the open structure, expanded and super wide interlayer spacing of MoS_2 nanoflowers.

Next, the electrochemical reversibility of the E-MoS_2/carbon fibers was further investigated by galvanostatic discharge/charge measurements, as shown in Fig. 4e and 4f. It can be noted that the E-MoS_2/carbon fibers exhibit a superior cycle performance, evidenced by that a high reversible capacity of 241 mA h g^{-1} can be retained after 700 cycles at a current density of 1 A g^{-1} which is nearly twice as large as that of the carbon fibers (121 mA h g^{-1}) and MoS_2/carbon fibers (117 mA h g^{-1}). Meanwhile, it can keep almost 100% Coulombic efficiency during the whole cycle process. And the capacity of 216 mA h g^{-1} still can be kept after 700 cycles even at a high current density of 2 A g^{-1}, fully demonstrating the high rate capacity and

excellent cycling stability of the as-made E-MoS_2/carbon fibers. Interestingly, the capacity of E-MoS_2/carbon fibers shows a slight increase during the cycle process due to the activation effects. This can also be evidenced by the EIS results shown in Fig. S9. It is noted that after the 250th cycle, the impedance of the battery decreases significantly compared with that before the first discharge because of the activation effects of electrode during cycle process. Moreover, after the 500th cycle, the impedance of the battery has no obvious change compared with that after the 250th cycle, indicative of the completion of the active effects [43]. Inspired by that, the longer-term cycle performance was tested at large current densities of 5 and 10 A g^{-1} (Fig. 4f). It is worth noting that the E-MoS_2/carbon fibers electrode delivers an ultralong cycle life up to 3000 cycles, which is comparable to the best cycle performance reported on MoS_2 electrodes (Fig. S11). The morphology and structure of E-MoS_2/carbon fibers after 500 cycles were also investigated, and the results were shown in Fig. S12. It can be clearly found that after 500 cycles, the electrode still maintains interconnected network structure (Fig. S12a). And the high-magnification SEM image (Fig. S12b) further shows that the MoS_2 nanoflowers keep the original morphology and still can be evenly anchored on the carbon fibers. This also further highlights the ability and potential of the E-MoS_2/carbon fibers as flexible SIBs electrodes.

The discharge/charge profiles without a distinct plateau region and the ultrahigh rate capability of the E-MoS_2/carbon fibers (Fig. 4d) are mainly attributed to the typical features of capacitive charge storage which occurs on the surface or near-surface of MoS_2 [44]. In order to evidence the contribution of capacitive charge storage in the present system, the CV measurements at different scan rates from 0.1 to 2 mV s^{-1} were carried out and the results are shown in Fig. 5a. The current response of the electrode material at different voltages obeys the following equation:

$$i = a \cdot v^b \tag{4}$$

where i is the current (mA), v is the scan rate (mV s^{-1}), and a and b are the appropriate values [45,46]. There are two well-defined conditions, namely $b=0.5$, it means a diffusion-controlled mechanism, which is indicative of a battery reaction process. On the other hand, $b=1$, it is representative of a surface capacitive response. In this case, the b values can classify and illustrate the electrochemical reaction behaviors. It can be noted from Fig. 5b that the cathodic and anodic b values for the E-MoS_2/carbon fibers at the voltage of 0.8 V are as high as 0.962 and 0.932 that are close to 1, indicating that the current response mainly originates from the surface capacitive reaction, rather than diffusion-controlled battery reaction. And the b values can be kept in the range of 0.9-1 at a large voltage range over 0.6 V (Fig. 5c). It is still as high as 0.88 even at the voltage of 0.01 V. Nevertheless, at the peak voltage of around 0.4 V, the contribution of diffusion-controlled battery reaction was more pronounced. More specifically, the surface capacitive contribution to the current response can be quantitatively detached based on the Eq. (5):

$$i = k_1 \cdot v + k_2 \cdot v^{1/2} \tag{5}$$

where k_1 and k_2 are appropriate values, and $k_1 \cdot v$ and $k_2 \cdot v^{1/2}$ correspond to the contributions of current response from the surface capacitive behavior and the diffusion-controlled battery reaction, respectively [47,48]. To get the values of k_1 and k_2, the Eq. (5) can be slightly rearranged to

$$i/v^{1/2} = k_1 \cdot v^{1/2} + k_2 \tag{6}$$

Then, the k_1 and k_2 can be obtained by plotting the $v^{1/2}$ *vs.* $i/v^{1/2}$ as shown in the Fig. S13. According to this methodology, the capacitive contribution for the current response can be detached and listed in Fig. 5d. The ratio of the capacitive contribution is positively correlated

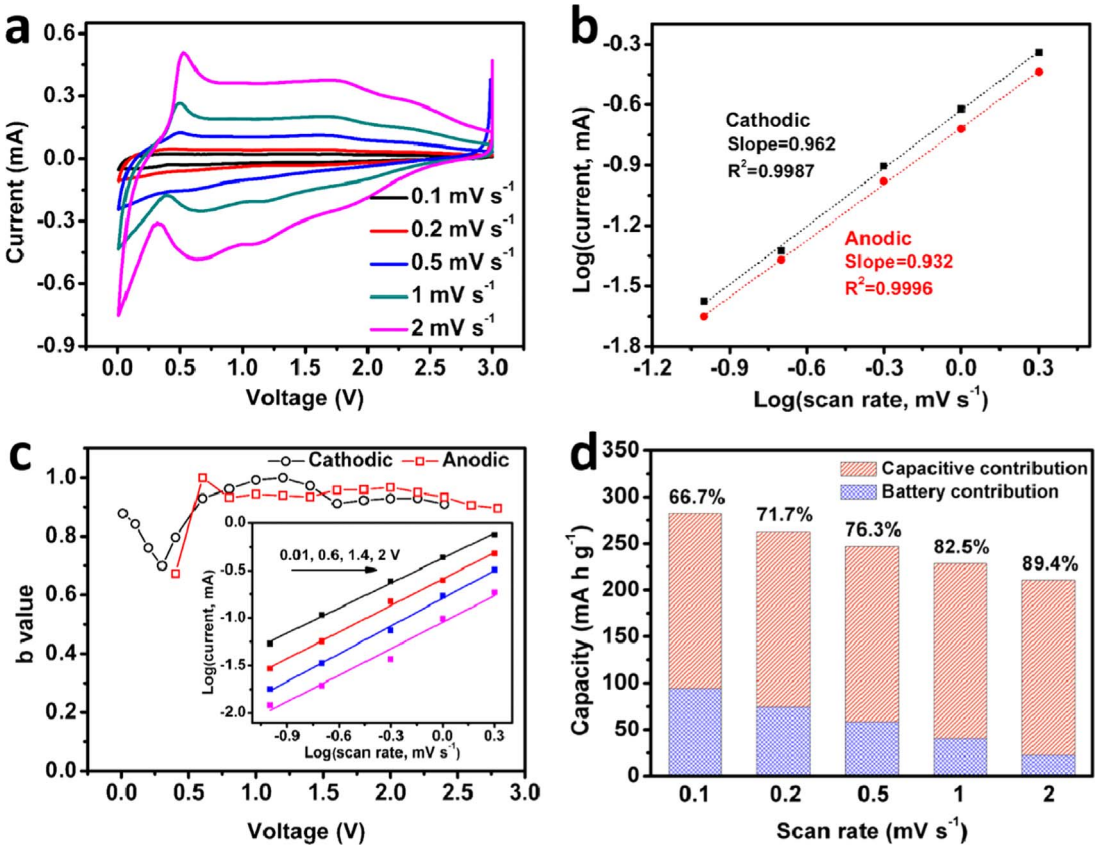

Fig. 5. (a) CV curves of the as-made E-MoS_2/carbon fibers at different scan rates. (b) Current *vs.* scan rate of the E-MoS_2/carbon fibers at the voltage of 0.8 V. (c) b values *vs.* battery voltage of the E-MoS_2/carbon fibers for cathodic and anodic scans, insert: current *vs.* scan rate of the E-MoS_2/carbon fibers at different voltages. (d) The capacities derived from capacitive contribution and battery contribution at different scan rates.

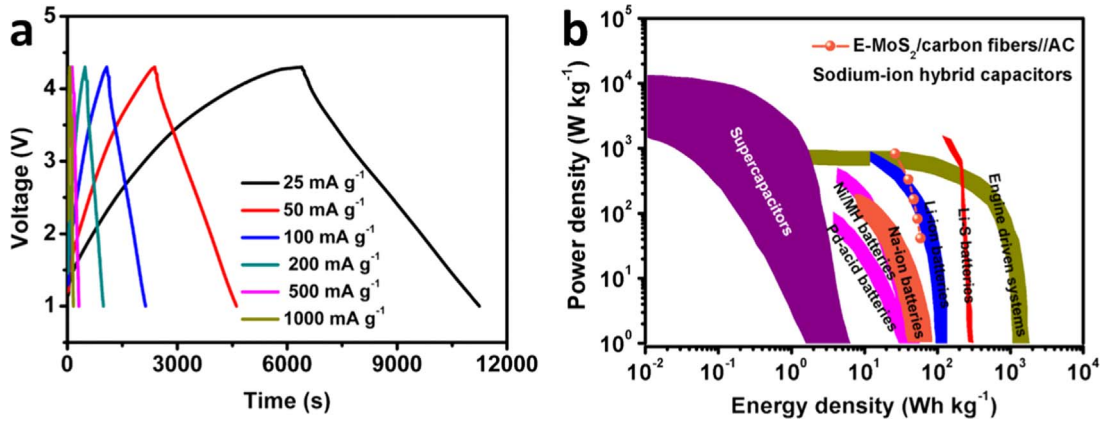

Fig. 6. (a) Galvanostatic charge/discharge profiles of the SHICs with E-MoS_2/carbon fibers//AC at different current densities. (b) Ragone plots of the SHICs with E-MoS_2/carbon fibers//AC (based on the total mass of electrode materials), and other energy storage devices.

with the scan rate, and it is even as high as 89.4% at a scan rate of 2 mV s^{-1}. The high capacitive contribution is mainly attributed to the unique structure of E-MoS_2/carbon fibers for the shortened ion diffusion pathways, the decreased ion diffusion barrier, the enhanced electron transfer, and the increased available and easily accessible active surface area.

With this information in mind, it is concluded that the capacitance contribution is dominated in the present system. Inspired by that, the feasibility of E-MoS_2/carbon fibers composite electrodes in SIHCs was also measured and evaluated. The coin-type asymmetric supercapacitors were assembled by using the composites as anodes, 1 M $NaClO_4$ in EC and DEC (volume ratio of 1:1) with 10 wt% FEC additive as the electrolyte, and commercial AC as cathodes. The calculation of current densities was based on the total mass of both anode and cathode active materials. The electrochemical performance was tested within the voltage window of 1.0–4.3 V. Upon charge, the Na^+ ions are stored in the anode by pseudocapacitive charge storage, meanwhile, and ClO_4^- ions are adsorbed on the AC cathode by means of double-layer charge storage. Fig. 6a shows representative galvanostatic charge/discharge profiles of SIHCs with E-MoS_2/carbon fibers//AC at different current densities. It can be found that charge/discharge profiles at all current densities are almost symmetric, indicative of a high Coulombic efficiency. The specific capacitance was calculated to be about 36.3 F g^{-1}, corresponding to an energy density of 54.9 Wh kg^{-1}. As shown in Fig. 6b, the SIHCs based on the E-MoS_2/carbon fibers//AC show a higher energy density and power density than these of current SIBs [49].

4. Conclusion

In summary, a simple and scalable strategy has been presented to configure the MoS_2 nanoflowers with expanded and super wide interlayer spacing (larger than 1.34 nm) supported on carbon fibers. The interlayer spacing that is the nearly twice as large as that of the original MoS_2 (theoretical value, 0.62 nm) is achieved for the as-made MoS_2, which will be in favor of decreasing the ion diffusion pathways and ion diffusion resistance, as well as increasing their available and accessible active surface area. When employed as the binder-free flexible anode for SIBs, the as-made E-MoS_2/carbon fibers exhibits an ultrahigh rate capacity of 104 mA h g^{-1} at a large current density of 20 A g^{-1} and an ultralong cycling stability up to 3000 cycles. The excellent rate performance is mainly attributed to the high pseudocapacitive charge storage of the E-MoS_2/carbon fibers derived from the unique structure for enhancing mass transport and electron transfer. The methodology of electrochemical separation further reveals that the ratio of the capacitive contribution even reaches as high as 89.4% at a scan rate of 2 mV s^{-1}. When employed as anode materials in SIHCs, the E-MoS_2/carbon fibers also deliver a higher energy density and power density than these of the current SIBs reported in literatures. This work presents a simple yet effective strategy for the configuration of flexible electrode and is expected to inspire the development of the pseudocapacitive charge storage for high-rate and long-life sodium storage.

Acknowledgements

This work was partly supported by the National Natural Science Foundation of China (NSFC, Nos. 21522601, U1508201, 21361162004), the Education Department of the Liaoning Province of China (No. T2013001), Natural Sciences and Engineering Research Council of Canada (NSERC), Canada Research Chair Program (CRC), Canada Foundation for Innovation (CFI), Ontario Research Fund (ORF), the University of Western Ontario, and Canada Light Source. C. Zhao was supported by the Chinese Scholarship Council.

Appendix A. Supporting information

Supplementary data associated with this article can be found in the online version at http://dx.doi.org/10.1016/j.nanoen.2017.08.030.

References

[1] J. Sun, H.-W. Lee, M. Pasta, H. Yuan, G. Zheng, Y. Sun, Y. Li, Y. Cui, Nat. Nanotechnol. 10 (2015) 980–985.
[2] Y.S. Yun, K.-Y. Park, B. Lee, S.Y. Cho, Y.-U. Park, S.J. Hong, B.H. Kim, H. Gwon, H. Kim, S. Lee, Y.W. Park, H.-J. Jin, K. Kang, Adv. Mater. 27 (2015) 6914–6921.
[3] B. Zhang, C.M. Ghimbeu, C. Laberty, C. Vix-Guterl, J.-M. Tarascon, Adv. Energy Mater. 6 (2016) 1501588.
[4] S. Kajiyama, L. Szabova, K. Sodeyama, H. Iinuma, R. Morita, K. Gotoh, Y. Tateyama, M. Okubo, A. Yamada, ACS Nano 10 (2016) 3334–3341.
[5] Y. Liu, H. Wang, L. Cheng, N. Han, F. Zhao, P. Li, C. Jin, Y. Li, Nano Energy 20 (2016) 168–175.
[6] C. Wu, Y. Jiang, P. Kopold, P.A. van Aken, J. Maier, Y. Yu, Adv. Mater. 28 (2016) 7276–7283.
[7] H. Hou, C.E. Banks, M. Jing, Y. Zhang, X. Ji, Adv. Mater. 27 (2015) 7861–7866.
[8] Y. Zhang, P. Zhu, L. Huang, J. Xie, S. Zhang, G. Cao, X. Zhao, Adv. Funct. Mater. 25 (2015) 481–489.
[9] C. Zhao, C. Yu, M. Zhang, H. Huang, S. Li, X. Han, Z. Liu, J. Yang, W. Xiao, J. Liang, X. Sun, J. Qiu, Adv. Energy Mater. 7 (2017) 1602880.
[10] H. Ye, L. Wang, S. Deng, X. Zeng, K. Nie, P.N. Duchesne, B. Wang, S. Liu, J. Zhou, F. Zhao, N. Han, P. Zhang, J. Zhong, X. Sun, Y. Li, Y. Li, J. Lu, Adv. Energy Mater. 7 (2017) 1601602.
[11] C. Zhang, X. Wang, Q. Liang, X. Liu, Q. Weng, J. Liu, Y. Yang, Z. Dai, K. Ding, Y. Bando, J. Tang, D. Golberg, Nano Lett. 16 (2016) 2054–2060.
[12] Y. Zheng, T. Zhou, C. Zhang, J. Mao, H. Liu, Z. Guo, Angew. Chem. Int. Ed. 55 (2016) 3408–3413.
[13] C. Wang, Y. Fang, Y. Xu, L. Liang, M. Zhou, H. Zhao, Y. Lei, Adv. Funct. Mater. 26 (2016) 1777–1786.
[14] C. Chen, Y. Wen, X. Hu, X. Ji, M. Yan, L. Mai, P. Hu, B. Shan, Y. Huang, Nat. Commun. 6 (2015) 6929.
[15] Q. Mahmood, S.K. Park, K.D. Kwon, S.-J. Chang, J.-Y. Hong, G. Shen, Y.M. Jung, T.J. Park, S.W. Khang, W.S. Kim, J. Kong, H.S. Park, Adv. Energy Mater. 6 (2016)

1501115.
[16] V. Augustyn, P. Simon, B. Dunn, Energy Environ. Sci. 7 (2014) 1597–1614.
[17] J.B. Cook, H.-S. Kim, Y. Yan, J.S. Ko, S. Robbennolt, B. Dunn, S.H. Tolbert, Adv. Energy Mater. 6 (2016) 1501937.
[18] D. Chao, C. Zhu, P. Yang, X. Xia, J. Liu, J. Wang, X. Fan, S.V. Savilov, J. Lin, H.J. Fan, Z.X. Shen, Nat. Commun. 7 (2016) 12122.
[19] Z. Chen, V. Augustyn, X. Jia, Q. Xiao, B. Dunn, Y. Lu, ACS Nano 6 (2012) 4319–4327.
[20] A.P. Cohn, K. Share, R. Carter, L. Oakes, C.L. Pint, Nano Lett. 16 (2016) 543–548.
[21] J.-K. Kim, Y. Kim, S. Park, H. Ko, Y. Kim, Energy Environ. Sci. 9 (2016) 1264–1269.
[22] S. Wang, L. Xia, L. Yu, L. Zhang, H. Wang, X.W. Lou, Adv. Energy Mater. 6 (2016) 1502217.
[23] J. Wang, J. Liu, H. Yang, D. Chao, J. Yan, S.V. Savilov, J. Lin, Z.X. Shen, Nano Energy 20 (2016) 1–10.
[24] X. Xie, Z. Ao, D. Su, J. Zhang, G. Wang, Adv. Funct. Mater. 25 (2015) 1393–1403.
[25] L. David, R. Bhandavat, G. Singh, ACS Nano 8 (2014) 1759–1770.
[26] G.S. Bang, K.W. Nam, J.Y. Kim, J. Shin, J.W. Choi, S.-Y. Choi, ACS Appl. Mater. Interfaces 6 (2014) 7084–7089.
[27] Y.-L. Ding, P. Kopold, K. Hahn, P.A. van Aken, J. Maier, Y. Yu, Adv. Mater. (2016) 7774–7782.
[28] T.S. Sahu, S. Mitra, Sci. Rep. 5 (2015) 12571.
[29] Y.-X. Wang, S.-L. Chou, D. Wexler, H.-K. Liu, S.-X. Dou, Chem. Eur. J. 20 (2014) 9607–9612.
[30] Y. Lu, Q. Zhao, N. Zhang, K. Lei, F. Li, J. Chen, Adv. Funct. Mater. 26 (2016) 911–918.
[31] X. Xie, T. Makaryan, M. Zhao, K.L. Van Aken, Y. Gogotsi, G. Wang, Adv. Energy Mater. 6 (2016) 1502161.
[32] S.H. Choi, Y.N. Ko, J.-K. Lee, Y.C. Kang, Adv. Funct. Mater. 25 (2015) 1780–1788.
[33] Z.-T. Shi, W. Kang, J. Xu, L.-L. Sun, C. Wu, L. Wang, Y.-Q. Yu, D.Y.W. Yu, W. Zhang, C.-S. Lee, Small 11 (2015) 5667–5674.
[34] J. Wang, C. Luo, T. Gao, A. Langrock, A.C. Mignerey, C. Wang, Small 11 (2015) 473–481.
[35] F. Cesano, S. Bertarione, A. Piovano, G. Agostini, M.M. Rahman, E. Groppo, F. Bonino, D. Scarano, C. Lamberti, S. Bordiga, L. Montanari, L. Bonoldi, R. Millini, A. Zecchina, Catal. Sci. Technol. 1 (2011) 123–136.
[36] D.H. Youn, J.-W. Jang, J.Y. Kim, J.S. Jang, S.H. Choi, J.S. Lee, Sci. Rep. 4 (2014) 5492.
[37] T. Yang, T. Qian, M. Wang, X. Shen, N. Xu, Z. Sun, C. Yan, Adv. Mater. 28 (2016) 539–545.
[38] Z. Jian, Z. Xing, C. Bommier, Z. Li, X. Ji, Adv. Energy Mater. 6 (2016) 1501874.
[39] J. Zhang, D.-W. Wang, W. Lv, S. Zhang, Q. Liang, D. Zheng, F. Kang, Q.-H. Yang, Energy Environ. Sci. 10 (2017) 370–376.
[40] Z. Liu, X.-Y. Yu, X.W. Lou, U. Paik, Energy Environ. Sci. 9 (2016) 2314–2318.
[41] L. Wang, X. Bi, S. Yang, Adv. Mater. 28 (2016) 7672–7679.
[42] C. Chen, H. Xu, T. Zhou, Z. Guo, L. Chen, M. Yan, L. Mai, P. Hu, S. Cheng, Y. Huang, J. Xie, Adv. Energy Mater. 6 (2016) 1600322.
[43] Z. Hu, L. Wang, K. Zhang, J. Wang, F. Cheng, Z. Tao, J. Chen, Angew. Chem. 126 (2014) 13008–13012.
[44] X. Wang, S. Kajiyama, H. Iinuma, E. Hosono, S. Oro, I. Moriguchi, M. Okubo, A. Yamada, Nat. Commun. 6 (2015) 6544.
[45] G.A. Muller, J.B. Cook, H.-S. Kim, S.H. Tolbert, B. Dunn, Nano Lett. 15 (2015) 1911–1917.
[46] Y. Wang, Z. Hong, M. Wei, Y. Xia, Adv. Funct. Mater. 22 (2012) 5185–5193.
[47] P. Yu, C. Li, X. Guo, J. Phys. Chem. C 118 (2014) 10616–10624.
[48] E. Lim, C. Jo, M.S. Kim, M.-H. Kim, J. Chun, H. Kim, J. Park, K.C. Roh, K. Kang, S. Yoon, J. Lee, Adv. Funct. Mater. 26 (2016) 3711–3719.
[49] C. Zhao, C. Yu, S. Liu, J. Yang, X. Fan, H. Huang, J. Qiu, Adv. Funct. Mater. 25 (2015) 6913–6920.

Changtai Zhao is currently a Ph.D. candidate in Prof. Jieshan Qiu's group at Dalian University of Technology, China. He was also a visiting student in Prof. Xueliang (Andy) Sun's Group at the University of Western Ontario, Canada, in 2016. He gained his Bachelor's degree from Department of Chemical Engineering, Qingdao University, China. His research interests focus on nanocarbon and advanced functional materials as well as their applications in energy conversion and storage, especially for Na/Li-ion batteries, Li-S batteries and Li-O_2 batteries.

Prof. Chang Yu received her Ph.D. degree from the School of Chemical Engineering at Dalian University of Technology (DUT) in 2008. She is currently a professor for School of Chemical Engineering at DUT. She was also a visiting professor at Rice University (USA) in 2015. Her research interests mainly focus on carbon coupled two-dimensional inorganic layered materials for energy storage and conversion applications.

Mengdi Zhang received her B.S. degree in Chemical Technology from Dalian University of Technology in 2012. Currently, she is a Ph.D. candidate at School of Chemical Engineering in Dalian University of Technology under the supervision of Prof. Jieshan Qiu. Her research mainly focuses on the design and synthesis of carbon-based nanomaterials for the application in supercapacitor and lithium secondary batteries.

Dr. Qian Sun is a postdoctoral fellow in Prof. Xueliang (Andy) Sun's Group at the University of Western Ontario, Canada. He received his B.S. degree in Chemistry in 2006, M.S. degree in Physical Chemistry in 2009, and Ph.D. degree in Applied Chemistry in 2013 at Fudan University, China, under the supervision of Prof. Dr. Zheng-Wen Fu on the study of Li-/Na-ion batteries and Na-air batteries. He joined Prof. Sun's group in 2013 and his current research interests focus on Na-air, Na-S, and Na-ion batteries as well as solid-state Li/Na batteries.

Shaofeng Li received his Bachelor's degree from the School of Chemistry and Chemical Engineering at Anhui University of Technology in 2014. He is currently a 1st year Ph.D. candidate in research group of Prof. Jieshan Qiu at Dalian University of Technology. His research interests mainly focus on rational design and optimization of carbon-based nanohybrids for energy storage and conversion application.

Dr. Mohammad Norouzi Banis is research engineer in Prof. Xueliang (Andy) Sun's group at University of Western Ontario, Canada. He received his Ph.D. degree in 2013 in Materials Science and Engineering from Western University, on the study of nanostructured low temperature fuel cells and application of x-ray absorption spectroscopy in energy related systems. His current research interests include study of metal ion, metal air and nanocatalysts via in-situ synchrotron based techniques.

Xiaotong Han is a Ph.D. student in Prof. Jieshan Qiu's group at Dalian University of Technology (DUT), China. He received his B.S. degree in Chemical Engineering and Technology in 2013 at Nanjing Tech University, China. He joined Prof. Qiu's group in 2013 and his current research interests focus on the design and fabrication of two-dimension nanohybrids derived from nanocarbons and transition metal compounds for energy storage and conversion devices including Li-ion batteries, supercapacitors as well as electrocatalysis.

Dr. Qiang Dong received his Ph.D. degree from the School of Chemical Engineering at Dalian University of Technology in 2016. His research interests mainly focus on design and optimization of carbon-based hybrids for capacitive deionization.

Juan Yang received his Bachelor's degree from the School of Chemical Engineering at Shenyang University of Chemical Technology in 2011, and he was a visiting student at Lawrence Berkeley National Laboratory (LBNL), USA. He is currently a Ph.D candidate in research group of Prof. Jieshan Qiu at Dalian University of Technology (DUT). His research interests mainly focus on design and optimization of carbon-based hybrids for energy storage and conversion application.

Dr. Gang Wang obtained his Ph.D. degree from the School of Environmental Science & Technology at Dalian University of Technology (DUT) in 2009. He is currently an associate professor of School of Chemical Engineering at DUT. He was also a visiting scholar at Oak Ridge Naitonal Lab (USA) in 2016. His research interests mainly focus on high performance capacitve deionization technology based on functional materials for water desalination and lithium extraction.

Prof. Xueliang (Andy) Sun is a Canada Research Chair in Development of Nanomaterials for Clean Energy, Fellow of the Royal Society of Canada and Canadian Academy of Engineering and Full Professor at the University of Western Ontario, Canada. Dr. Sun received his Ph.D. in materials chemistry in 1999 from the University of Manchester, UK, which he followed up by working as a postdoctoral fellow at the University of British Columbia, Canada and as a Research Associate at L'Institut National de la Recherche Scientifique (INRS), Canada. His current research interests are focused on advanced materials for electrochemical energy storage and conversion, including electrocatalysis in fuel cells and electrodes in lithium-ion batteries and metal-air batteries.

Prof. Jieshan Qiu obtained his Ph.D. degree in the School of Chemical Engineering at Dalian University of Technology (DUT) in 1990. He was also a visiting professor at Pennsylvania State University (USA), West Virginia University (USA), and the University of Reading (UK). He was appointed to a Cheung-Kong Distinguished Professor in 2009. He is a professor of School of Chemical Engineering and director of the Carbon Research Laboratory at DUT. His current research includes functional carbon nanotubes, graphene, carbon nanohybrids, and their applications (energy conversion and storage, capacitive deionization technique, etc.).